Analytica Chimica Acta 1169 (2021) 338629

Contents lists available at ScienceDirect

Analytica Chimica Acta

journal homepage: www.elsevier.com/locate/aca

Label-free tapered optical fiber plasmonic biosensor

Thakshila Liyanage, Meimei Lai, Gymama Slaughter*

Old Dominion University, Frank Reidy Research Center for Bioelectrics, Bioelectronics Laboratory, Department of Electrical and Computer Engineering, Norfolk, VA, 23508, USA

HIGHLIGHTS

- Demonstrated a label-free ultrasensitive gold nanoparticle laminated TOF plasmonic biosensor.
- Successfully detected five panels of microRNAs simultaneously with unprecedented selectivity.
- Synergistic response derived from evanescent field exciting surface plasmon resonance.
- Extended linear dynamic range 1 fM to 100 nM.
- Achieved sub-femtomolar limit of detection for the panel of microRNAs.

GRAPHICAL ABSTRACT

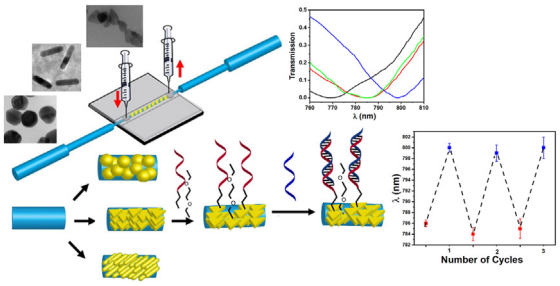

ARTICLE INFO

Article history:
Received 13 March 2021
Received in revised form
4 May 2021
Accepted 6 May 2021
Available online 11 May 2021

Keywords:
Biosensor
microRNA
Tapered optical fibers
Evanescent field
Surface plasmon resonance

ABSTRACT

We designed and fabricated a novel label-free ultrasensitive tapered optical fiber (TOF) plasmonic biosensor that successfully detected a five panel of microRNAs with good selectivity. The biosensing platform integrates three different metallic nanoparticles: gold spherical nanoparticles (AuNPs), gold nanorods (AuNRs), and gold triangular nanoprisms (AuTNPs) laminated TOF to enhance the evanescent mode. The dip in the intensity profile of the transmission spectrum corresponded to the specific wavelength of the nanoparticle. The AuTNPs laminated TOF was found to exhibit the highest refractive index sensitivity and was therefore used to assay the panel of microRNAs. Single stranded DNA probes were self-assembled on the AuTNPs TOF plasmonic biosensors to achieve the highest sensitivity from the formation of hydrogen bonds between the ssDNAs and the target microRNAs. Experimentally, we observed that by measuring the spectral shifts, a limit of detection (LOD) between 103 aM and 261 aM for the panel of microRNAs can be achieved. Additionally, the ssDNA layer immobilized on the TOF plasmonic biosensor resulted in an extended dynamic range of 1 fM – 100 nM. In human serum solution, clinically relevant concentration of the panel of microRNAs were successfully detected with a LOD between 1.097 fM to 1.220 fM. This is the first report to demonstrate the applicability of our TOF plasmonic biosensor approach to detect a panel of microRNAs. This simple yet highly sensitive approach can provide a high-throughput and scalable sensor for detecting and quantifying large arrays of microRNAs, thereby expanding the applications of biosensors.

1. Introduction

MicroRNAs are small non-coding RNAs with ~19–22 nucleotides, which are capable of modulating gene activity at the post-transcriptional level. In addition, microRNA expression profiles

* Corresponding author.
E-mail address: gslaught@odu.edu (G. Slaughter).

https://doi.org/10.1016/j.aca.2021.338629
0003-2670/

have become useful biomarkers for diagnostics and prognosis of cancers and other diseases because of their outstanding stability in biological samples (plasma, serum, urine etc.) [1,2]. Quantitative measurement of microRNAs can serve as an early diagnostic tool. The current techniques for the detection and quantification of microRNA employs microarrays and qRT-PCR; however, these techniques involve the use of sophisticated instrumentation and sample preparation steps [3]. Fluorescence [4], electronic and electrochemical [5,6], microresonator [7,8], and nanopore-based techniques [9–11] have been reported and can provide portability and label-free sensing. Due to the availability of miniaturized optical spectrum analyzers, it is now possible to develop low-cost portable surface plasmon resonance (SPR) biosensors using optical fibers for the detection of biological or chemical analytes.

We study optical fiber-based sensing approach because of their stability in harsh environment and at high temperatures [12]. They are highly biocompatible and not receptive to electromagnetic interference [13]. The biosensing mechanism is dependent on optical transduction mechanisms for detecting target biomolecules [14]. The light of an optical fiber propagates based on the total internal reflection (TIR) principle. When light is fully reflected inside the core, no electromagnetic field propagates towards the cladding [15]. However, the electromagnetic waves can slightly penetrate the lower refractive index cladding. This light propagation is parallel to the interface of core-cladding, and decays exponentially with the distance from the interface [15]· [16]. Thereby, an evanescent wave is created when the electromagnetic field crosses the interface at a penetration depth (d_p). When d_p is smaller than the cladding thickness, the interaction between the propagating light and the external medium is negligible and limits its application in biosensing. Therefore, the cladding material is partially or entirely removed to access the evanescent field and enable its interaction with the external medium, wherein the d_p changes as a function of the coupled cladding mode and the external refractive index [16].

To this end, we enhanced the sensitivity of the evanescent field by coupling with metallic nanoparticle that laminates tapered optical fibers (TOFs) to create a novel label-free TOF plasmonic biosensor with an improved LOD without any signal amplification. The use of a TOF allows the excitation of the surface plasmon waves in the supporting metallic layer of the fiber surface. Localized surface plasmon resonance (LSPR) is the collective oscillation of electrons on the metallic nanostructure that is excited by the incident photons at the resonant frequency [17,18], thereby resulting in an enhanced and tunable electromagnetic fields, light absorption and scattering based on the physical and elemental parameters of the nanostructure [17,19]. Although LSPR based technologies have been reported to detect a wide range of biomolecules (e.g., proteins, microRNAs, enzymes etc.) with high sensitivity [17,20–24], some LSPR based sensors require an amplification strategy to achieve an improved limit of detection (LOD) [17,22–24].

Here we demonstrated an ultrasensitive TOF plasmonic biosensor through the coupling of various gold nanoparticles: gold spherical nanoparticles (AuNPs), gold nanorods (AuNRs), and gold triangular nanoprisms (AuTNPs) that laminates the TOFs. The laminated TOFs were functionalized with single stranded DNA (ssDNA) capture probes and polyethylene glycol thiol spacer biomolecules. Upon microRNA hybridization with the ssDNA functionalized TOF, the spectral shift with nm scale. Without any amplification, the AuTNPs demonstrated good sensitivity towards the panel of microRNA compare to other optical biosensors immobilized with ssDNA for the detection of other molecules [25–27]. In addition, high throughput microRNA detection was achieved wherein five samples were analyzed. This TOF plasmonic biosensor demonstrated the ability to detect target microRNA with high sensitivity.

2. Materials and methods

Materials. Gold (III) chloride trihydrate ($HAuCl_4.3H_2O$) solution, chloro(triethyl phosphine) gold (I) (Et_3PAuCl, 97%), polymethylhydrosiloxane (PMHS, M_n = 1700-3300), cetyl trimethyl ammonium bromide (CTAB) and triethylamine (TEA, 98%) were procured from Sigma-Aldrich. ACS grade acetonitrile (CH_3CN, 99.9%), ethanol (22 proof) (3-aminopropyl)-triethoxysilane (APTES, 94%), RBS35 detergent, sodium citrate trihydrate, RNase H (100U) enzyme, and sodium borohydride were procured from Thermo Scientific and used as received. ssDNA and microRNA listed in Table S1 and Table S2 were procured from IDT.

Synthesis of Gold Nanoparticles (AuNPs). 2.8 mL of gold (III) chloride trihydrate solution was added to 80 mL of ultrapure water (Barnstead™ Smart2Pure™ Water Purification System) and stirred in an ice bath. Then 1.0 mL of 0.01 M $Na_3C_6H_5O_7$ was added to reaction mixture and stirred in an ice bath for 30 min. In the interim, 0.1 M $NaBH_4$ solution was prepared and cooled in an ice bath separately. Afterward, 1.5 mL of $NaBH_4$ was injected to the gold solution and stirred. Rapid reduction of gold (III) was observed via color change of yellow to wine red. The solution was stored at 4 °C overnight.

Synthesis of Gold Nanorods (AuNRs). A seed-mediated method using CTAB as passivating ligands was employed for synthesizing AuNRs. Briefly, a seed solution was prepared by adding 7.5 mL of 100 mM CTAB solution to 20 mL scintillation glass vial followed with the addition of 250 μL of 10 mM $HAuCl_4.3H_2O$ under constant stirring for 5 min 10 mM $NaBH_4$ was added to the solution to result in a light brown colored solution. 48 μL of this seed solution was added to the growth solution comprising of 28 mL of 100 mM CTAB, 2 mL of 10 mM $HAuCl_4.3H_2O$, and 400 μL of 10 mM $AgNO_3$ and 220 μL of 100 mM ascorbic acid at room temperature. The solution was kept in a water bath overnight to achieve a dark pink colored solution. The CTAB capped AuNRs were redissolved in ultrapure water containing 1 mM PEG4-SH for ligand exchange under constant stirring for over 24 h. The obtained PEG functionalized AuNRs were centrifuged and redissolved in ultrapure water.

Synthesis of Gold Triangular Nanoprisms (AuTNPs). $Et_3PAu(I)Cl$ (0.010 g) was dissolved in 20 mL CH_3CN and stirred at medium speed for 5–10 min at room temperature. Then 0.019 mL of TEA was added to the reaction mixture and heated gradually to 40 °C. At 40 °C, 0.3 mL of PMHS was added and allowed to react for approximately 3 h. Then the reaction mixture was centrifuged at 5000 rpm for 1 min. After removing the unreacted PMHS the reaction mixture was precipitated out via centrifugation and redissolved in ultrapure water. The formation of the various gold nanostructures was confirmed by UV–vis absorption spectroscopy.

TOF Plasmonic Biosensor Fabrication. Although chemical etching of the cladding material using hazardous acid has been reported [27], here we report a simple and straightforward approach to partially remove the cladding material by fabricating tapered optical fibers (TOFs). Following previously reported works, we designed a tapering rig system using the flame brushing technique to form a thin tapered optical fiber structure [25–27]. Approximately 1 m length of a single mode optical fiber was obtained. The polymer coating on a 3 cm region of the 125 μm diameter fiber to be tapered is stripped out, cleaned with acetone, and fixed in the fiber holders of our home built tapering rig system. Using the flame brushing technique, the 3 cm glass region was exposed to the butane heat source to soften the glass while the fiber tails were pulled in opposite directions to form the TOF with a waist diameter of 5 μm. This technique is adaptable for the fabrication of adiabatic tapered fiber with excellent optical and physical properties [28]. As a result, the channel spectrum features can be observed in the transmission spectrum due to the d_p of the evanescent field.

The TOFs were mounted on Teflon channel chips that consisted of a 48 mm × 6 mm x 2 mm (*l* x *w* x *d*) cell to contain the analyte molecules within the tapered region for profiling of the bound analyte (Scheme 1A). The chip surface was seal by a layer of polydimethylsiloxane (PDMS) leaving the inlets and outlets open. Eight of these TOF devices can be integrated onto a single Teflon chip utilizing laser fabrication processes to realize fast-multiplexed and high-throughput biosensors.

The TOF fiber was separately laminated with three different Au nanoparticles: AuNPs, AuNRs, and AuTNPs (Scheme 1B-E). The TOFs were cleaned in a 10% (v/v) aqueous RBS 35 detergent solution at 90 °C for 30 min. The TOFs were thoroughly rinsed with ultrapure deionized water and immersed in a solution mixture of concentrated hydrochloric acid and methanol (1:1 v/v) for 30 min. Afterward, the TOFs were washed with copious amount of ultrapure water and dried under air for 3 h prior to use. The dried TOFs were then incubated in a solution of 15% APTES in ethanol purged with nitrogen for 30 min. The TOFs were then rinsed with ethanol to remove unbound APTES. After rinsing, the TOFs were dried in air and finally incubated in 2 mL of the prepared Au nanostructure solutions for 1h to form a coating of Au nanostructures on to the TOF.

Afterward, the laminated TOFs were separately incubated in the respective complementary 5 μM ssDNA solution prepared in 1 μM PBS (ssDNA-$(CH_2)_n$-X:SH (where X is the complementary base pairs for the target microRNA)) and 1 mM polyethylene glycol thiol (PEG-SH) spacer molecules to prevent non-specific binding on the TOF and allowed to react overnight (Scheme F). The ssDNA functionalized laminated TOF was rinsed with PBS buffer to remove loosely bound reactants. Upon conjugating the ssDNA probes with the Au nanoparticles on the TOF surface, we observed a red shift in the TOF signal as shown in Scheme 1H (red curve). Finally, various concentrations of the target microRNA were prepared and 800 μL of the microRNA solution was delivered to the biosensor and allowed to hybridize for 4 h. Once the hybridization between the immobilized ssDNA probes and the target microRNAs occurs at the surface of the TOF (Scheme 1G), the Au nanoparticles enhance the electromagnetic field coupling range and thus resulted in additional red shifting of the optical signal as shown in Scheme 1H (blue curve).

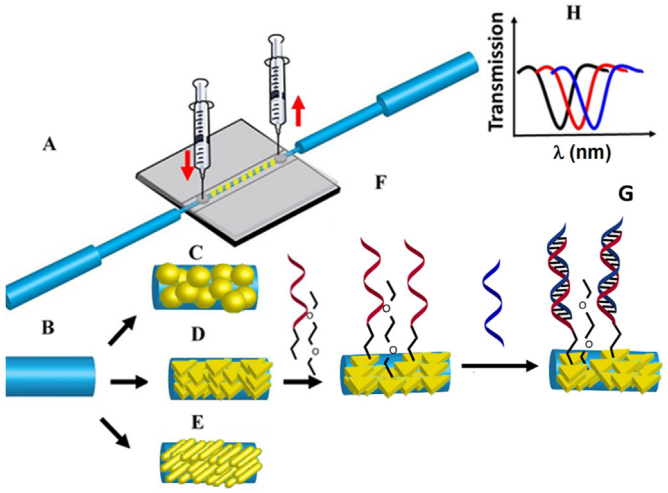

Scheme 1. (A) Schematic representation of the designed and fabricated TOF plasmonic biosensor, (B) functionalization of TOF with 3-aminopropyl-triethoxysilane (APTES), (C) Gold (Au) nanoparticles (AuNPs) laminated TOF, (D) Au triangular nanoparticles (AuTNPs) laminated TOF, and (E) Gold nanorods (AuNRs) laminated TOF, (F) ssDNA and PEG-SH functionalized TOF, (G) hybridization with target microRNA, and (H) illustration of transmission spectrum of the functionalization steps: Au nanostructure decorated TOF (black curve, ssDNA immobilization (red curve), and upon hybridization (blue curve).

Absorption and extinction spectra in the range of 400–1000 nm were collected with a Spectra Max M5 microplate reader from Molecular Devices, LLC. Extinction spectra of the prepared AuNPs, AuNRs, and AuTNPs in the solution phase were measured to determine the LSPR peak position (λ_{LSPR}). For the RI sensitivity studies, all transmission spectra were obtained in aqueous glucose solutions for all nanostructures using Superk Compact Supercontinuum Lasers in the range of 450–2400 nm. All transmission spectra of the TOF plasmonic biosensors were recorded in phosphate buffered saline (PBS) at room temperature after all reactions reached equilibrium using a compact Czerny-Turner CCD spectrometer (CCS200, Thorlabs Inc.). The silanized TOF was used as a blank spectrum for the study. The λ_{peak} maximum was determined through curve fitting using Origin and ΔTransmission was derived by taking the difference between the transmittance of the TOF plasmonic biosensors before and after hybridization with the target microRNA. The obtained spectra were normalized by using smooth function in Origin. Accordingly, adjacent averaging method was utilized with 200 points of window. The LOD was determined by using the Z value of the blank (Z = mean +3σ, σ = standard deviation), which was obtained from three ΔTransmission measurements.

3. Results and discussion

Tapered Optical Fiber (TOF) Plasmonic Biosensor Platform. The low-cost TOF was constructed using a flame brushing technique to soften the glass optical fiber for elongation. The tapering progress and waist diameter of the TOF was monitored using a power meter and a microscope to evaluate the power loss and diameter of the fabricated TOF, respectively. The 3 cm region of the fabricated TOF was transitioned from a diameter of 125 μm to a taper waist diameter of ~5 μm. Fig. 1A–C shows the scanning electron microscopy (SEM) micrographs of snapshots of the TOF fabrication. The evanescent wave *dp* has been reported to be enhanced when the waist diameter is less than 10 μm with a decreased in the transmitted power [28]. This technique has proved to be flexible and fast for the fabrication of tapered fiber.

Prior to laminating the TOF with Au nanoparticles (AuNPs, AuNRs and AuTNPs), the TOF was mounted onto a Teflon microchannel chip. The waist region of the TOF was cleaned and then coated with the desired Au nanoparticles via silanization with 3-aminopropyl-triethoxysilane (APTES)/ethanol solution to activate the silane group on the TOF and provide a self-assembled monolayer containing amine group for coupling to the Au nanoparticles. Subsequently, the solution containing the desired Au nanoparticles was delivered to the waist region of TOF to obtain Au nanoparticles laminated on the surface of the TOF. The optical power transmitted through the TOF decreased by ~80%. This decreased is ascribed to the absorption losses by the Au nanoparticles during the process. Fig. 1D shows the SEM micrograph of the TOF laminated with AuTNPs. The AuTNPs formed a layer of nanoparticles distributed around the fiber. This distribution of the nanoparticles provides for a sensitive optical interaction with the surrounding media.

TOF Plasmonic Bulk Refractive Index Sensing. The transmission electron microscopy (TEM) micrographs of the three TOF plasmonic sensors are showed in Fig. 2A–C. The average size of the nanoparticles is 40 ± 1.2 nm (AuNPs), 40 ± 0.8 nm (AuNRs), and 38 ± 1.5 nm edge length (AuTNPs). Fig. 2D shows LSPR profile of the three different nanoparticles in water, where AuNPs, AuNRs, and AuTNPs exhibited λ_{LSPR} of 530 nm, 840 nm, and 770 nm, respectively. A supercontinuum laser (450 nm to 2400 nm) was then used to couple the light into the TOF plasmonic sensor and a spectrometer was connected at the other end to collect the signal. The

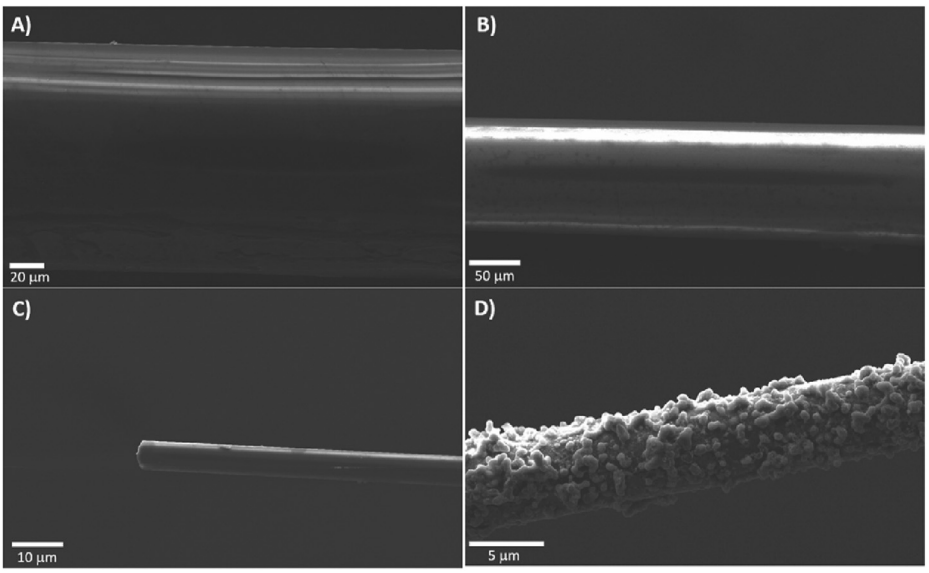

Fig. 1. Scanning electron micrographs (SEM) of (A) single mode fiber ($\varphi = 125$ μm), (B) fiber after stripping the buffer coating ($\varphi = 100$ μm), (C) tapered optical fiber (TOF) with fiber waist of approximately 5 μm over a 2.5 mm length fiber region, (D) gold triangular nanoparticles (AuTNPs) laminated tapered optical fiber (TOF).

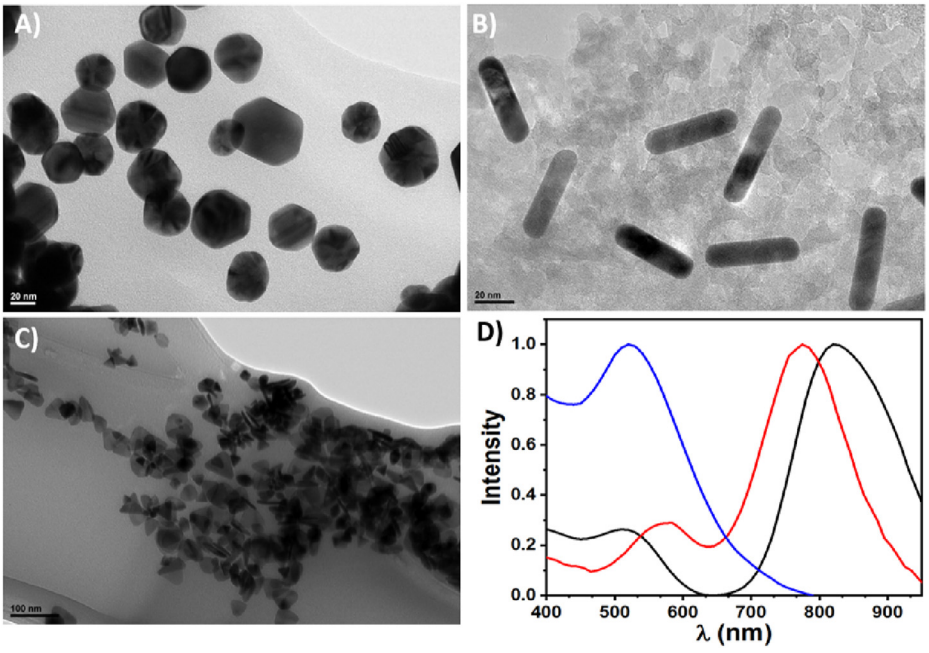

Fig. 2. Transmission electron microscopy (TEM) micrographs of (A) AuNPs (B) AuNRs, and (C) AuTNPs. (D) UV−visible extinction spectra of AuNPs (blue, $\lambda_{LSPR} = 530$ nm), Au NRs (black, $\lambda_{LSPR} = 840$ nm), and AuTNPs (red, $\lambda_{LSPR} = 770$ nm). (For interpretation of the references to color in this figure legend, the reader is referred to the Web version of this article.)

solid phase spectral shift, $\Delta\lambda_{peak}$, was obtained upon laminating the TOF with the Au nanoparticles. We observed a dip in the optical transmission spectrum due to the presence of Au nanoparticles at 550 nm, 840 nm, and 770 nm for AuNPs, AuNRs, and AuTNPs, respectively. This is attributed to the excitation of the surface plasmon waves by the evanescent waves generated in the TOF. On average, a 20 nm red shift is observed for AuNPs, while no shifts were observed for the AuNRs and AuTNPs decorated TOF when compare to the λ_{LSPR} obtained with UV−vis spectroscopy. Masterson at el. reported similar red shifted λ_{LSPR} for AuNPs upon binding to a substrate [11]. The spectral shifts observed with the transmission spectra are found to be very sensitive to refractive index (RI) changes.

Since the refractive indices and densities of aqueous solutions of "sugar" have been well studied [29], we then study the effect of different glucose concentrations on the changes in the RI and the corresponding wavelength induced by the three TOF plasmonic biosensors. The glucose concentration is varied from 0 wt% (deionized water only) to 40 wt% glucose in 10 wt% increments and the optical response is monitored since the nanoparticles are responsive to the refractive changes of their bulk environment. Each glucose characterization was performed in triplicates and sensors exhibited a good repeatability wherein the triplicate spectra were almost superimposed. The sensor was thoroughly

rinsed with deionized water after each characterization. As illustrated in Fig. 3A–D, the transmission spectra obtained for the Au laminated TOF showed a gradual red-shift with increasing glucose concentration, whereas the unfunctionalized non-laminated TOF showed an increase in transmission intensity as the result of background RI effect. An increase in RI of the surrounding medium is clear for each of the Au laminated TOF plasmonic sensor in different glucose concentrations in relation to 0 wt% glucose (black curve). The obtained data exhibited the same trend described for a spherical particle optical response using Mie theory [30]. The bulk sensitivities of AuNPs, AuNRs and the AuTNPs laminated TOFs were 114 nm/RIU 184 nm/RIU, and 263 nm/RIU, respectively as shown in Fig. 4. The highest sensitivity was achieved with the AuTNPs TOF plasmonic sensor, which was expected because the AuTNPs exhibit a geometry with sharp edges compare to the AuNPs and AuNRs TOF plasmonic sensors. The sharp edges on the AuTNPs leads to the generation of an enhanced localized SPR phenomenon that is attributed to the electromagnetic field around the sharp tip, edges, and corners of the AuTNPs due to the polarization effects when compared to the curved surfaces such as those seen in nanorods and spherical nanoparticles [17]. Upon comparison to the unfunctionalized non-laminated TOF, the sensitivity of the TOF is enhanced when laminated with Au nanoparticles (e.g., AuNPs, AuNRs, and AuTNPs) because of the electromagnetic field coupling enhancement generated near the sensing region. In addition, it has been noted that the shift in λ_{peak} is due to the increase in effective RI of the tapered region in close contact with the plasmonic metallic particles [27]. This TOF plasmonic biosensor provides a platform for low-cost fabrication and integration into microfluidics for high throughput assays without compromising the biosensing efficiency and have some advantages over LSPR biosensors, wherein the spectral shift ($\Delta\lambda_{peak}$) in the transmission spectra can be used to additionally monitor RI.

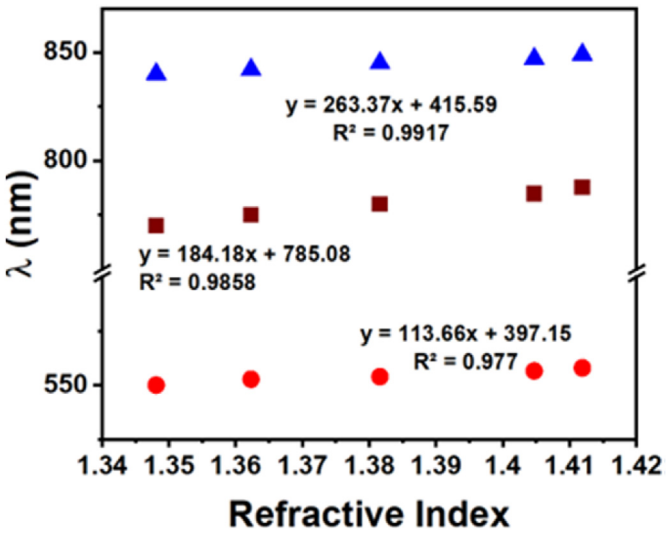

Fig. 4. Calibration plots of AuNPs (•), AuNRs (■), and AuTNPs (▲) TOF plasmonic sensors. aqueous glucose solutions.

MicroRNA Sensing. The $\Delta\lambda_{peak}$ of the TOF plasmonic biosensor was evaluated during the ssDNA surface modification and the hybridization of target microRNA in phosphate buffer saline (PBS). The PBS incubation solution contained 5 μM ssDNA probe to target mircoRNA let 7a. The ssDNA probe was reacted with 0.1 M tris(2-carboxyethyl) phosphine (TCEP) solution for an hour to reduce disulfide to thiol. And 1 mM PEG-SH was added as a spacer molecule to prevent non-specific binding. The resulting ssDNA probe and

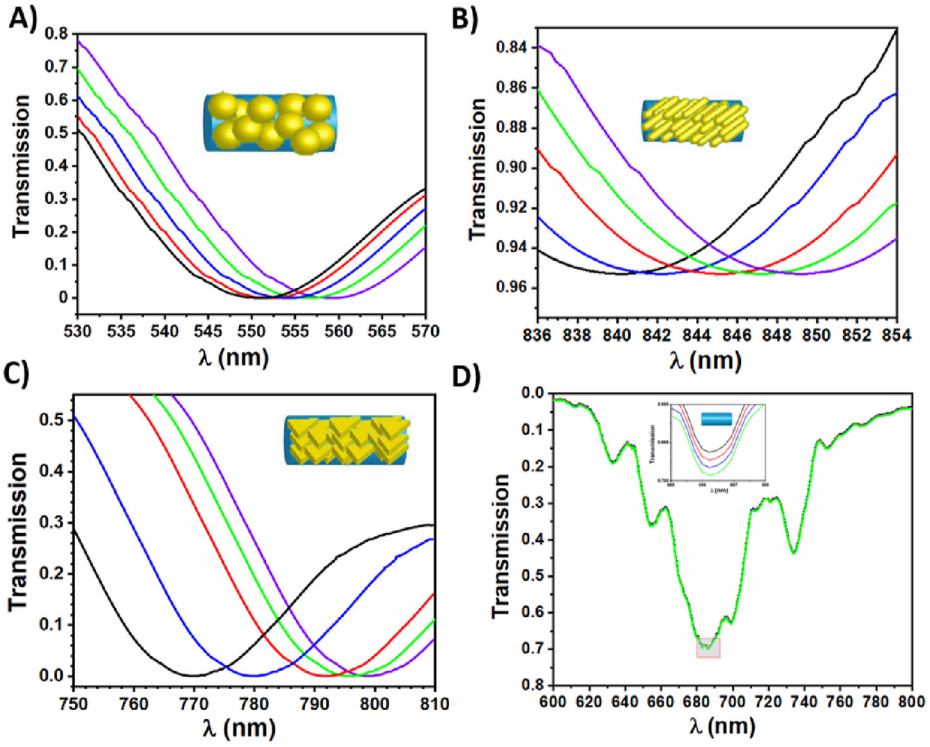

Fig. 3. Refractive index sensitivity characterization. Normalized transmission spectra of gold laminated TOF plasmonic sensors: (A) Au SPs, (B) Au NRs, and (C) AuTNPs in different concentration of glucose. 0 wt% glucose (black curve), 10 wt% glucose (blue curve), 20 wt% glucose (red curve), 30 wt% glucose (green curve), 40 wt% glucose (purple curve). (D) transmission spectra of the unfunctionalized non-laminated TOF in different concentration of glucose. (For interpretation of the references to color in this figure legend, the reader is referred to the Web version of this article.)

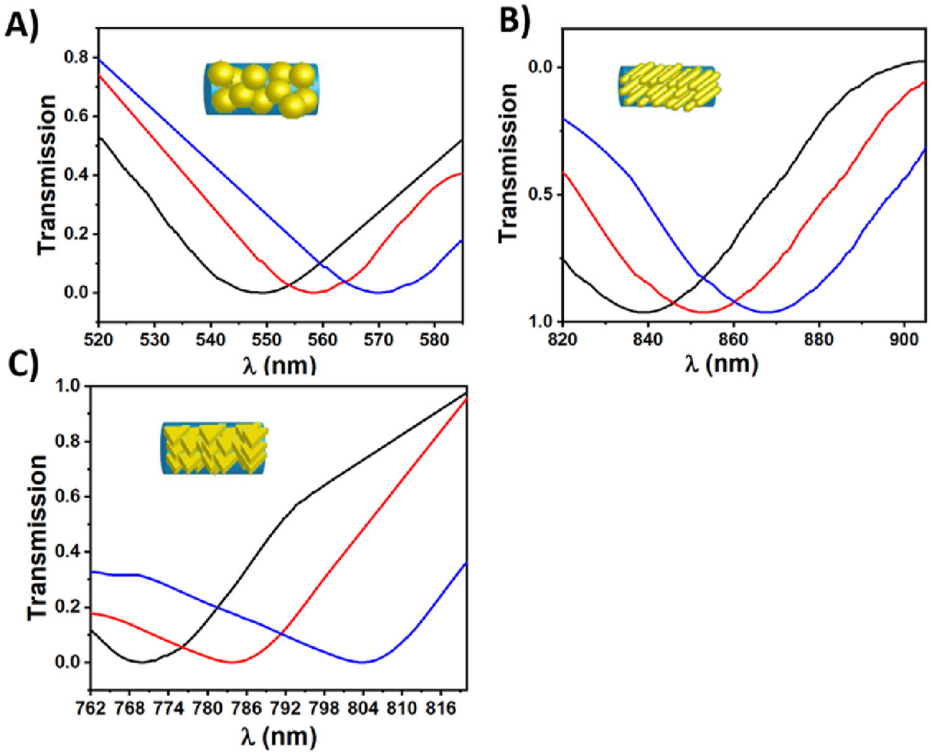

Fig. 5. Transmission spectra of (A) AuNPs (B) AuNRs, and (C) AuTNPs decorated TOFs (black curve), after ssDNA and PEG modification (red curve), and after hybridization of ssDNA with target microRNA. (For interpretation of the references to color in this figure legend, the reader is referred to the Web version of this article.)

PEG-SH (1:1000) functionalized TOF serves as the TOF plasmonic biosensor ready for the detection of the target microRNA molecule. Upon conjugating the DNA and PEG molecules to the TOF plasmonic biosensor surface, approximately a 10 nm, 13 nm, and 15 nm red shift was observed in the λ_{peak} of AuNPs, AuNRs, and AuTNPs as shown in Fig. 5A–C. Subsequently, the detection process commenced with the hybridization between the DNA-functionalized TOF and the microRNA let-7a (1 nM) at the surface of the TOF plasmonic biosensor. A 11.5 nm, 15 nm, and 21 nm red shifts in the λ_{peak} was observed for AuNPs, AuNRs, and AuTNPs plasmonic biosensor, respectively (Fig. 5A–C). The functionalization and hybridization steps collectively induce a substantial red

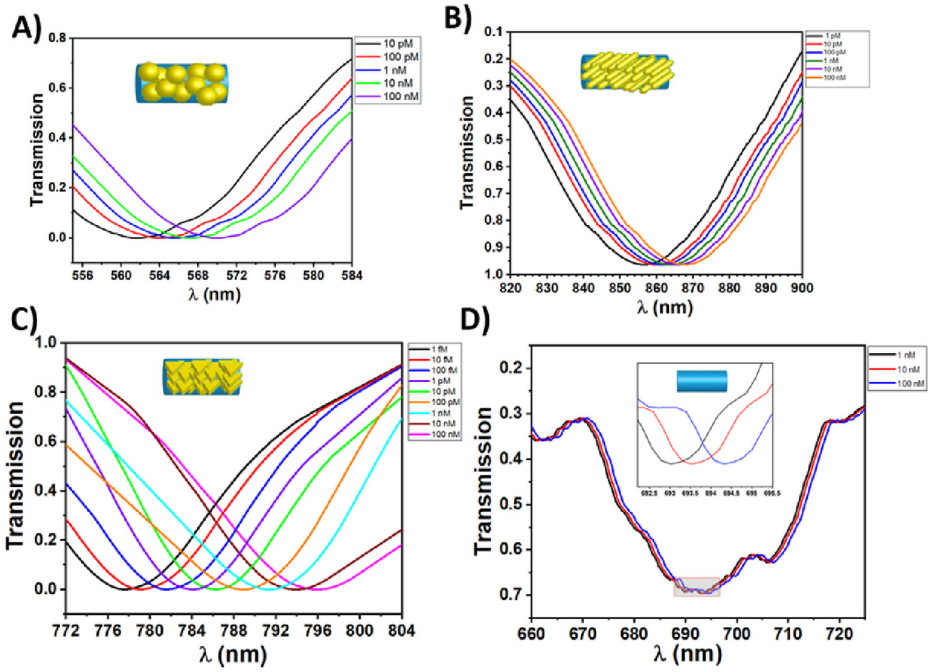

Fig. 6. Normalized transmission spectra of the differently laminated TOF plasmonic biosensor: (A) AuNPs (B) AuNRs, (C) AuTNPs, and (D) ssDNA functionalized non-laminated TOF.

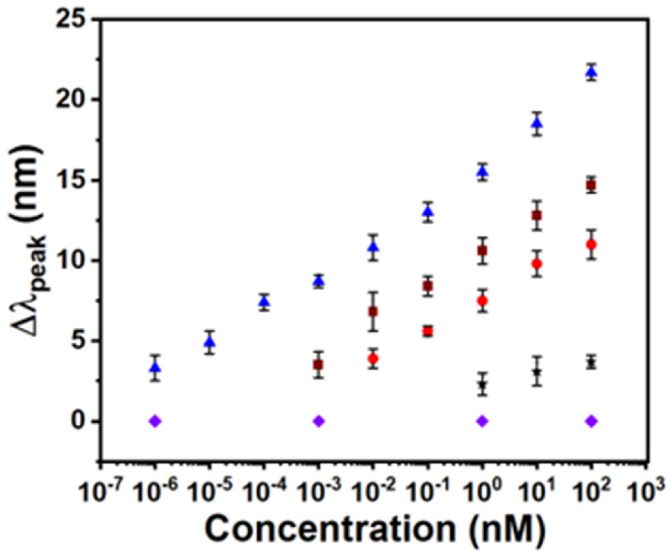

Fig. 7. Corresponding calibration curves for TOF plasmonic biosensors functionalized with AuNPs (•), AuNRs (■) TNPs, AuTNPs (▲), ssDNA functionalized non-laminated TOF (★), and unfunctionalized non-laminated TOF (◆).

shift in the λ_{peak} and these large shifts are attributed to significant enhancement in the TOF plasmonic biosensor sensitivity upon the formation of hydrogen bonds between the ssDNAs and the TOF plasmonic biosensor surface and between the ssDNAs and the target microRNAs.

Accordingly, Fig. 6A–D shows the λ_{peak} red shifted with increasing concentrations of microRNA let-7a. Fig. 7 depicts the calibration curves where the $\Delta\lambda_{peak}$ is shown to correlate linearly with logarithm of the microRNA concentration levels. The TOF plasmonic biosensors exhibited a dynamic range of 10 pM–100 nM with a sensitivity of 0.93 nm/nM for AuNPs (•), 1 pM–100 nM with a sensitivity of 0.95 nm/nM for AuNRs (■), and 1 fM – 100 nM with a sensitivity of 0.98 nm/nM for AuTNPs (▲) and a limit of detection (LOD) of 51.8 pM, 95.1 fM, and 121 aM microRNA let-7a was observed for AuNPs, AuNRs and AuTNPs, respectively. The ssDNA functionalized non-laminated TOF was prepared by taking the concentrated hydrochloric acid and methanol (1:1 v/v) cleaned and dried TOFs and incubating the TOF in the respective complementary 5 μM ssDNA with 0.1 M TCEP solution for an hour. After which, 1 mM PEG-SH solution was added and allowed to react overnight followed by rinsing in PBS buffer. Upon hybridization of the immobilized ssDNA probes and the target microRNAs at the surface of the TOF, the ssDNA functionalized non-laminated TOF (★) exhibited a narrowed dynamic range of 1 nM to 100 nM with a relatively poor sensitivity of 0.25 nm/nM and an LOD of 161 μM microRNA let-7a. Although, the unfunctionalized non-laminated TOF showed an increase in transmission intensity as the result of background RI effect, it exhibited no $\Delta\lambda_{peak}$ response at all. This further illustrates that the lamination of TOF with Au nanoparticles have synergic effects that enhance the electromagnetic field coupling noticeably and results in nearly a 4-fold increase in sensitivity and aM limit of detection microRNA.

Furthermore, both the bulk refractive index sensitivity and microRNA detection studies revealed that AuNPs showed comparatively satisfactory sensitivity and LOD when compared to AuNRs and AuTNPs. The AuTNPs based TOF plasmonic biosensor exhibited large sensing volume that resulted in the highest sensitivity, extended dynamic range and lowest LOD. Thus, AuTNPs based plasmonic biosensor was used to evaluate the panel of microRNAs. Fig. S1A and Table 1 depict the obtained calibration curves and corresponding regression equations illustrating the ultrasensitive response for the detection of ultra-low concentration of microRNAs in PBS. A sensitivity and LOD of 0.98 nm/nM and 121 aM, 0.90 nm/nM and 168 aM, 0.92 nm/nM and 103 aM, 0.97 nm/nM and 201 aM, and 0.91 nm/nM and 261 aM for microRNA let 7a, 141, let 7c, 200 and 21 were obtained, respectively. Following the characterization of the panel of microRNAs, the serum matrix effect of the TOF plasmonic biosensor was evaluated using 40% human serum spiked with predefined volume of 1 μM target microRNA to achieve 1 fM – 100 nM microRNA in human plasma without any amplification. As shown in Fig. S1B, the results illustrate that the PEG spacer

Table 1
AuTNPs TOF biosensor regression characteristics.

		Equation	R^2	LOD	SD
PBS	Let *7a*	y = 0.9764ln(x)+ +16.03	0.9872	121 aM	0.6111
	mRNA 141	y = 0.9026ln(x)+ +14.95	0.9903	168 aM	0.6111
	Let 7c	y = 0.9171ln(x) + 15.65	0.9817	103 aM	0.6111
	mRNA 21	y = 0.9084ln(x) + 15.91	0.9819	261 aM	0.4778
	mRNA 200	y = 0.9714ln(x) + 15.91	0.9827	201 aM	0.6444
Human Serum	Let 7a	y = 0.9706ln{x) + 14.56	0.9940	1.22 fM	0.4778
	mRNA 141	y = 0.9301ln(x) + 13.88	0.9848	1.10 fM	0.6111
	Let 7c	y = 0.9887ln(x) + 14.89	0.9952	0.972 fM	0.6111
	mRNA 200	y = 0.9605ln(x) + 14.39	0.9763	1.18 fM	0.6444
	mRNA21	y = 1.0054ln(x) + 14.99	0.9876	1.01 fM	0.6111

SD - vtandard deviation.

Table 2
Comparison of label-free microRNA optical sensors.

microRNA Type	Sample Source	Method	Linear Range	LOD	Referense
Let7a	Synthetic RNA	MZI	2 nM - 20 μM	212 pM	[7]
10a and 10b	Culture media	I SPR	1 fM - 10 nM	83aM	[20]
10a and 10b	Human plasma	I SPR	100 aM - 1 nM	32 aM-0.15pM	[21]
21 and let-7a	Clinical urine samples	MZI	IfM –1 pM	1 fM	[31]
10b and 21	Human plasma	I SPR	50 fM - 100 nM	23-35 fM	[32]
21 and 155	Synthetic RNA	I SPR	10 aM- 10pM	10aM	[33]
let7a,let7c,21,141, and 200	Human serum	TOF	1 fM - 100 nM	1 fM	This work

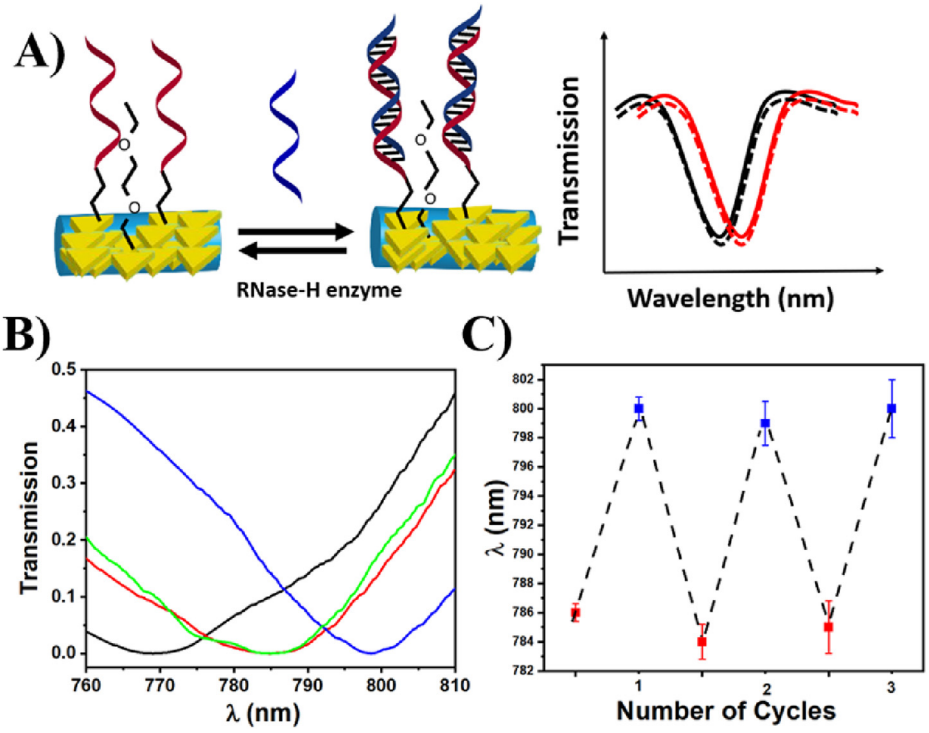

Fig. 8. (A) Schematic illustration of TOF plasmonic biosensor regeneration. (B) Normalized transmission spectrum of a reversible cycle: Black – AuTNPs TOF plasmonic biosensor, Red – immobilized ssDNA probe, Blue – DNA-RNA duplex (hybridization with 1 nM microRNA let 7a), and Green – RNase H treatment. C) Three full cycles of surface regeneration. (For interpretation of the references to color in this figure legend, the reader is referred to the Web version of this article.)

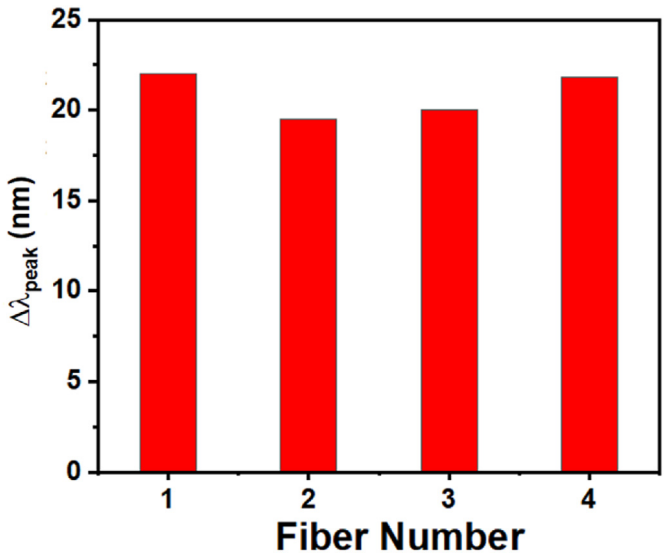

Fig. 9. Comparison of four TOF plasmonic biosensors quantified in triplicates for the detection of microRNA-141.

molecule efficiently minimized non-specific binding to the surface of the TOF plasmonic biosensor, where a similar dynamic range of 1 fM – 100 nM microRNA was observed. Table 1 shows slightly higher sensitivities and higher LODs of 0.97 nm/nM and 1220 aM, 0.93 nm/nM and 1097 aM, 0.99 nm/nM and 972 aM, 0.96 nm/nM and 1181 aM, and 1.01 nm/nM and 1014 aM for microRNA let 7a, 141, let 7c, 200 and 21 were obtained, respectively. The higher LODs are attributed to the inherent negative effects caused by serum proteins. The $\Delta\lambda_{peak}$ was observed to be highly correlated with the microRNA concentration levels. Thereby indicating that the fabricated TOF plasmonic biosensors can be used to detect a microRNAs in biological samples.

Table 2 provides a comparison of the fabricated TOF plasmonic biosensor with existing optical biosensors to detect microRNA molecules. Similar microRNA molecules have been sensed using a variety of optical biosensors including LSPR based biosensors with an LOD ranging from 212 pM–10 aM and a dynamic range from 10 aM–100 nM. The fabricated TOF plasmonic biosensor exhibited better LOD compared to the sensors reported by Liang et al. and Joshi et al. [7,32]. However, others have reported sub-attomolar LODs using the LSPR method [20,21]. This may be the result of the sensitivity of the devices. The LODs of our fabricated TOF plasmonic biosensors are overall comparable to previously reported optical biosensor (LOD = 1 fM) [31].

Selectivity and Regenerative Characteristics. The selectivity of the TOF plasmonic biosensor was evaluated to ensure that the biosensor was selective towards the target miRNA molecule. The AuTNPs TOF plasmonic biosensor (black curve) was incubated in a solution of complimentary ssDNA probe to target mircoRNA let 7a and a $\Delta\lambda_{peak}$ was detected at 782 nm as shown in Fig. S2 (blue curve). The ssDNA functionalized AuTNPs TOF plasmonic biosensor was then introduced to a solution mixture of 100 nM equimolar non-complimentary microRNA sequences (microRNA let 7c, microRNA 200, microRNA 141, and microRNA 21), and the biosensor showed no shift in the $\Delta\lambda_{peak}$ (red curve). However, upon exposure to the microRNA let7a solution, binding the target molecules, a shift in the $\Delta\lambda_{peak}$ (green curve) was observed, thereby illustrating the selectivity and specificity of biosensor to detect the target miRNA, let 7a using complementary ssDNA probe to microRNA let 7a. These results demonstrate that the TOF plasmonic biosensor enables highly sensitive and selective, label-free detection of target microRNA over background effect produce by related

microRNA molecules. Furthermore, the selectivity test provided a unique opportunity for evaluating the specificity of the TOF plasmonic biosensor towards the target microRNA let 7a. microRNA let 7a and let 7c exhibit one nucleotide mismatch at the 15th position in their entire sequence, and microRNA let 7c was not detected by the fabricated TOF plasmonic biosensor with complimentary ssDNA probe to target mircoRNA let 7a, thereby illustrating the high specificity of the TOF plasmonic biosensor.

Since the obtained calibration plot exhibited similar dynamic range, we investigated the binding isotherms of the complementary ssDNA to the targeted microRNAs in serum by fitting the data to the Hill equation using GraphPad Prism as shown in Fig. S3. We observed an effective dissociation constant, k_d, of 3.521 ± 0.4778 nM, 4.465 ± 0.6111 nM, 7.895 ± 0.6111 nM, 1.399 ± 0.6444 nM, and 0.1142 ± 0.6111 nM for microRNA let 7a, 141, 21, 200, and let 7c, respectively. MicroRNA concentrations up to 100 nM were employed since these biomarkers are present in picomolar concentrations in patient's serum. The highest microRNA concentration resulted in ca. 20 nm shift. The binding curve shows a saturation point beyond 30 nm shift with micromolar concentrations. Since the highest microRNA concentration used was 100 nM similar linear range were observed. Table S3 provides the dissociation constant and Hill coefficient (h) and adjusted R^2 values for the Hill equation (Equation S1) for all five microRNAs for all concentration range. The k_d provides the binding affinity between the complementary ssDNA and the target microRNA. This in turn relates to the sensitivity and selectivity of the assay towards target analyte, thereby enabling the exploration of specificity and sensitivity of ssDNA to enable low microRNA concentration binding. Additionally, the given Hill coefficient of all binding curves were less than 1 and that indicates the binding of a target microRNA to their target receptor decreases the binding affinity of subsequent receptors to assure the high specificity of binding.

Regeneration of a biosensor surface is an important characteristic that enables the same biosensor to be used for multiple assays. As shown in Fig. 8A, the regenerative aspects of the TOF plasmonic biosensor with ssDNA complimentary probe for let 7a and the PEG spacer molecule is illustrated. Fig. 8B shows the biosensor response after incubation in a 1 nM microRNA-let 7a (blue curve). A total red shift in the λ_{peak} of approximately 29.5 nm was observed from the capture ssDNA attachment to the hybridization with microRNA-let 7a. The hybridized DNA-RNA duplex on the TOF plasmonic biosensor surface was then incubated in 10 units RNase H enzyme solution for 2 h to selectively unhybridized the DNA-RNA duplex. The obtained transmission spectrum (green curve) shows an average 14 nm blue shift in the λ_{peak} response. Thereby, the TOF plasmonic biosensor returned to its original λ_{peak} position (red curve) for ssDNA complimentary probe for let 7a and the PEG spacer molecule. We successfully demonstrated that the TOF plasmonic biosensor surface can be regenerated and re-used two times as shown in Fig. 8C.

The reproducibility of the biosensor was determined using four similarly prepared TOF plasmonic biosensors as depicted in Fig. 9. The sensors response in the presence of 100 nM microRNA 141 were quantified in triplicates. An average $\Delta\lambda_{peak}$ of 20.84 nm with a low standard deviation of 1.09 was obtained for the four biosensors. The relative standard deviation of 5.23% confirms small variation in the biosensors' response. These results demonstrate good functionality and repeatability of the TOF plasmonic biosensor in detecting target microRNA.

4. Conclusion

We successfully demonstrated the fabrication of an innovative label-free ultrasensitive TOF plasmonic biosensor using Au nanoparticle laminated TOF. We reported bulk refractive index sensitivity of 263 nm/RIU for the AuTNPs TOF plasmonic sensor. The feasibility of the TOF plasmonic biosensor for the detection of a panel of microRNAs was evaluated. We demonstrated attomolar LODs without sample amplification. The aM LOD was achieved because of the evanescent waves exciting the localized surface-plasmon resonance to enhance the electromagnetic field coupling of the biosensor, thereby resulting in a noticeable dip in the transmission spectrum and red shifting with increasing target microRNA concentrations. The TOF plasmonic biosensor exhibited ultrasensitivity to the quantitative detection of the target microRNAs. In addition, the TOF plasmonic biosensor demonstrated excellent selectivity towards target microRNA and no significance response was observed in the presence of other microRNAs. This low-cost AuTNPs TOF plasmonic biosensor showed fM LOD for the microRNA in 40% human serum over a dynamic range of 1 fM – 100 nM with a slightly higher sensitivity. The TOF plasmonic biosensor signifies a unique approach for detecting microRNAs.

CRediT authorship contribution statement

Thakshila Liyanage: Writing – original draft, Formal analysis. **Meimei Lai:** performed the experiment. **Gymama Slaughter:** revised the manuscript, conceived the project.

Declaration of competing interest

The authors declare that they have no known competing financial interests or personal relationships that could have appeared to influence the work reported in this paper.

Acknowledgment

This work was supported by National Science Foundation under Grant 1921363.

Appendix A. Supplementary data

Supplementary data to this article can be found online at https://doi.org/10.1016/j.aca.2021.338629.

References

[1] B. Ortiz-Quintero, Cell-free microRNAs in blood and other body fluids, as cancer biomarkers, Cell Prolif 49 (3) (2016) 281–303.
[2] C. Eyileten, Z. Wicik, S. De Rosa, D. Mirowska-Guzel, A. Soplinska, C. Indolfi, I. Jastrzebska-Kurkowska, A. Czlonkowska, M. Postula, MicroRNAs as diagnostic and prognostic biomarkers in ischemic stroke-a comprehensive review and bioinformatic analysis, Cells 7 (12) (2018) 249.
[3] A. Git, H. Dvinge, M. Salmon-Divon, M. Osborne, C. Kutter, J. Hadfield, P. Bertone, C. Caldas, Systematic comparison of microarray profiling, real-time PCR, and next-generation sequencing technologies for measuring differential microRNA expression, Rna 16 (5) (2010) 991–1006.
[4] Z. Zhang, Y. Wang, Y. Li, D. Yu, H. Chen, Y. Cai, W. Fang, Z. Yang, Y. Ji, Y. Guan, Y. Chu, C. Xu, Portable fluorescence-based microRNA detection system based on isothermal signal amplification technology, Biotechnol. Appl. Biochem. 66 (1) (2019) 82–90.
[5] W. Cheng, J. Ma, P. Cao, Y. Zhang, C. Xu, Y. Yi, J. Li, Enzyme-free electrochemical biosensor based on double signal amplification strategy for the ultrasensitive detection of exosomal microRNAs in biological samples, Talanta 219 (2020) 121242.
[6] Y. Chu, R. Wu, G.-C. Fan, A.-P. Deng, J.-J. Zhu, Enzyme-free photoelectrochemical biosensor based on the Co-sensitization effect coupled with dual cascade toehold-mediated strand displacement amplification for the sensitive detection of MicroRNA-21, ACS Sustain. Chem. Eng. 6 (9) (2018) 11633–11641.
[7] L. Liang, L. Jin, Y. Ran, L.-P. Sun, B.-O. Guan, Interferometric detection of microRNAs using a capillary optofluidic sensor, Sensor. Actuator. B Chem. 242 (2017) 999–1006.
[8] Y.-H. Wang, K.-J. Huang, X. Wu, Y.-Y. Ma, D.-L. Song, C.-Y. Du, S.-H. Chang, Ultrasensitive supersandwich-type biosensor for enzyme-free amplified

microRNA detection based on N-doped graphene/Au nanoparticles and hemin/G-quadruplexes, J. Mater. Chem.B: Mater.Biol. Med. 6 (14) (2018) 2134–2142.
[9] X.-L. Huo, H. Yang, W. Zhao, J.-J. Xu, H.-Y. Chen, Nanopore-Based Electrochemiluminescence for Detection of MicroRNAs via duplex-specific nuclease-assisted target recycling, ACS Appl. Mater. Interfaces 9 (38) (2017) 33360–33367.
[10] M. Kamal Masud, M.N. Islam, M.H. Haque, S. Tanaka, V. Gopalan, G. Alici, N.-T. Nguyen, A.K. Lam, M.S.A. Hossain, Y. Yamauchi, M.J.A. Shiddiky, Gold-loaded nanoporous superparamagnetic nanocubes for catalytic signal amplification in detecting miRNA, Chem. Commun. 53 (58) (2017) 8231–8234.
[11] T. Yasui, Y. Baba, Nanobiodevice-based single cell analysis and single biomolecule analysis, Bunseki Kagaku 64 (6) (2015) 413–419.
[12] S. Korposh, S.W. James, S.-W. Lee, R.P. Tatam, Tapered optical fibre sensors: current trends and future perspectives, Sensors 19 (10) (2019) 2294.
[13] N. Sabri, S.A. Aljunid, M.S. Salim, S. Fouad, Fiber Optic Sensors: Short Review and Applications, vol. 204, Springer Series in Materials Science, 2015, pp. 299–311 (Recent Trends in Physics of Material Science and Technology).
[14] X.-d. Wang, O.S. Wolfbeis, Fiber-optic chemical sensors and biosensors (2015-2019), Anal. Chem. 92 (1) (2020) 397–430.
[15] C.A.J. Gouveia, J.M. Baptista, P.A.S. Jorge, Refractometric optical fiber platforms for label free sensing, Current Developments in Optical Fiber Technology (2013) 345–373.
[16] R. Correia, S. James, S.W. Lee, S.P. Morgan, S. Korposh, Biomedical application of optical fibre sensors, J. Opt. 20 (7) (2018), 073003/1-073003/25.
[17] M. Lai, G. Slaughter, Label-free MicroRNA optical biosensors, Nanomaterials 9 (11) (2019) 1573.
[18] M. Sui, S. Kunwar, P. Pandey, J. Lee, Strongly confined localized surface plasmon resonance (LSPR) bands of Pt, AgPt, AgAuPt nanoparticles, Sci. Rep. 9 (1) (2019) 1–14.
[19] J.J. Mock, R.T. Hill, Y.-J. Tsai, A. Chilkoti, D.R. Smith, Probing dynamically tunable localized surface plasmon resonances of film-coupled nanoparticles by evanescent wave excitation, Nano Lett. 12 (4) (2012) 1757–1764.
[20] G.K. Joshi, S. Deitz-McElyea, T. Liyanage, K. Lawrence, S. Mali, R. Sardar, M. Korc, Label-free nanoplasmonic-based short noncoding RNA sensing at attomolar concentrations allows for quantitative and highly specific assay of MicroRNA-10b in biological fluids and circulating exosomes, ACS Nano 9 (11) (2015) 11075–11089.
[21] T. Liyanage, A.N. Masterson, H.H. Oyem, H. Kaimakliotis, H. Nguyen, R. Sardar, Plasmoelectronic-based ultrasensitive assay of tumor suppressor microRNAs directly in patient plasma: design of highly specific early cancer diagnostic technology, Anal. Chem. 91 (3) (2019) 1894–1903.
[22] A.N. Masterson, T. Liyanage, C. Berman, H. Kaimakliotis, M. Johnson, R. Sardar, A novel liquid biopsy-based approach for highly specific cancer diagnostics: mitigating false responses in assaying patient plasma-derived circulating microRNAs through combined SERS and plasmon-enhanced fluorescence analyses, Analyst 145 (12) (2020) 4173–4180.
[23] L. Zhang, Y. Xu, X. Jin, Z. Wang, Y. Wu, D. Zhao, G. Chen, D. Li, X. Wang, H. Cao, Y. Xie, Z. Liang, A circulating miRNA signature as a diagnostic biomarker for non-invasive early detection of breast cancer, Breast Canc. Res. Treat. 154 (2) (2015) 423–434.
[24] E.E. Rufino-Paiomares, F.J. Reyes-Zurita, J.A. Lupianez, P.P. Medina, MicroRNAs as oncogenes and tumor suppressors, MicroRNAs in Medicine (2014) 223–243.
[25] Y.M. Kamil, M.H. Abu Bakar, M.H. Yaacob, A. Syahir, H.N. Lim, M.A. Mahdi, Dengue E protein detection using a graphene oxide integrated tapered optical fiber sensor, IEEE J. Sel. Top. Quant. Electron. 25 (1) (2019) 7201008/1–7201008/8.
[26] S. Kumar, B.K. Kaushik, R. Singh, N. Chen, Q.S. Yang, X. Zhang, W. Wang, B. Zhang, LSPR-based cholesterol biosensor using a tapered optical fiber structure, Biomed. Opt Express 10 (5) (2019) 2150–2160.
[27] L. Singh, G. Zhu, R. Singh, B. Zhang, W. Wang, B.K. Kaushik, S. Kumar, Gold nanoparticles and uricase functionalized tapered fiber sensor for uric acid detection, IEEE Sensor. J. 20 (1) (2020) 219–226.
[28] C. Beres, F.V.B. de Nazaré, N.C.C. de Souza, M.A.L. Miguel, M.M. Werneck, Tapered plastic optical fiber-based biosensor—tests and application, Biosens. Bioelectron. 30 (1) (2011) 328–332.
[29] C.F. Snyder, A.T. Hattenburg, Refractive indices and densities of aqueous solutions of invert sugar, NBS Monograph (United States), No. 64 (1963) 1–4.
[30] I. Niskanen, V. Forsberg, D. Zakrisson, S. Reza, M. Hummelgård, B. Andres, I. Fedorov, T. Suopajärvi, H. Liimatainen, G. Thungström, Determination of nanoparticle size using Rayleigh approximation and Mie theory, Chem. Eng. Sci. 201 (2019) 222–229.
[31] Q. Liu, Y. Shin, J.S. Kee, K.W. Kim, S.R.M. Rafei, A.P. Perera, X. Tu, G.-Q. Lo, E. Ricci, M. Colombel, et al., Mach–Zehnder interferometer (MZI) point-of-care system for rapid multiplexed detection of microRNAs in human urine specimens, Biosens. Bioelectron. 71 (2015) 365–372.
[32] G.K. Joshi, S. Deitz-McElyea, M. Johnson, S. Mali, M. Korc, R. Sardar, Highly specific plasmonic biosensors for ultrasensitive MicroRNA detection in plasma from pancreatic cancer patients, Nano Lett. 14 (2014) 6955–6963.
[33] T. Xue, W. Liang, Y. Li, Y. Sun, Y. Xiang, Y. Zhang, Z. Dai, Y. Duo, L. Wu, K. Qi, et al., Ultrasensitive detection of miRNA with an antimonene-based surface plasmon resonance sensor, Nat. Commun. 10 (2019) 28.